Knockdown of Dnmt1 links Gene body DNA methylation to regulation of gene expression and maternal-zygotic transition in the wasp *Nasonia*

Deanna Arsala[1,2], Xin Wu[3], Soojin V. Yi[3], and Jeremy A. Lynch[1]

[1] Department of Biological Sciences, University of Illinois at Chicago, Chicago IL

[2] Dept. of Ecology & Evolution, University of Chicago, Chicago IL

[3] School of Biological Sciences, Georigia Institute of Technology, Atlanta GA

Abstract

Gene body methylation (GBM) is an ancestral form of DNA methylation whose role in development has remained unclear. Unlike vertebrates, DNA methylation is found exclusively in gene bodies in the wasp *Nasonia vitripennis*, which provides a unique opportunity to interpret the role of GBM in development. We confirmed that parental RNAi (pRNAi) knockdown of DNMT1 (*Nv-Dnmt1a*) in *Nasonia* leads to embryonic lethality and failures in cellularization and morphogenesis. Using whole-genome bisulfite sequencing, we found a widespread loss of GBM in *Nv-Dnmt1a* pRNAi embryos. Using RNAseq, we found that methylated genes that lost GBM in the pRNAi samples were exclusively downregulated during zygotic genome activation. Unexpectedly, nearly all affected unmethylated genes were up-regulated after pRNAi. Lack of proper clearance of mRNAs and abnormal activation drive this up-regulation, indicating critical roles for *Nv-Dnmt1a* and GBM in the maternal-zygotic transition (MZT) in the wasp, despite their absence in *Drosophila*.

Background

The maternal-zygotic transition (MZT) is an essential stage in multicellular eukaryotic development and represents the transition of developmental control <u>from</u> maternal genome products provided to the egg during oogenesis <u>to</u> the products of newly formed zygotic genome [1, 2]. A major hallmark of the handover to zygotic control is the coordination of the highly regulated decay of maternal mRNAs with the activation of transcription from the zygotic genome.

46 The interactions between the maternal and zygotic genome have been
47 most comprehensively demonstrated in the insect model *Drosophila*
48 *melanogaster*. Maternal transcript destabilization is carried out in part by
49 maternally deposited mRNAs encoding RNA binding proteins (RBPs) such as
50 *smaug* and *brain tumor* (*brat*) [3, 4]. These factors are aided by the transcription
51 factor Zelda (Zld), which promotes miRNA expression that further destabilize
52 maternal transcripts. Under normal circumstances Zld also increases chromatin
53 accessibility and helps activate thousands of zygotic genes to their proper level [5,
54 6, 7]. However, if clearance of maternal transcripts is impeded, the zygotic genome
55 is not properly activated. Thus, disruption of either zygotic genome activation, or
56 maternal transcript clearance leads to embryonic lethality. In both cases death is
57 due to failures in the earliest developmental events that are dependent on the
58 zygotic genome: cellularization of the syncytial blastoderm, and gastrulation [5, 8] .
59 Most of the strategies for regulating the *D. melanogaster* ZGA (e.g.,
60 histone modification, chromatin packaging, action of miRNAs, mRNA
61 degradation), and many of the molecules involved, are conserved throughout the
62 animals [9]. However, *D. melanogaster* lacks a major class of genomic regulation,
63 in the form of methylation of cytosines in CpG dinucleotides (CpG methylation) [10,
64 11]. CpG methylation is crucial for regulating gene expression in most complex
65 eukaryotes [12, 13], and has a significant role in regulating the MZT in many species
66 [14, 15]. Thus, its absence in *D. melanogaster*, and in the other major invertebrate
67 model system *C. elegans*, makes it difficult to elucidate the molecular
68 mechanisms of DNA methylation in early development.

69 CpG methylation is catalyzed by DNA methyltransferases 1 and 3
70 (DNMT1 and DNMT3), which are conserved and ancient components of the
71 eukaryotic genomic toolkit [16], but have been lost in Dipterans, including *D.*
72 *melanogaster* [17, 18]. However, both DNMT1 and 3 orthologs are found in many
73 other insect taxa including hemimetabolous insects [19] and within the
74 holometabolous lineage Hymenoptera [20, 21, 22, 23].
75 The most well understood functional impact of CpG methylation,
76 elucidated from studies of mammalian model system, is in silencing gene
77 expression via methylation of cis-regulatory sequences, particularly of normally
78 unmethylated clusters of CpGs (CpG islands) [13, 24]. However it is becoming clear
79 that cis-regulatory regulation at CpG islands is not a ubiquitous mechanism [25]. A
80 more universal, and likely ancestral [20, 26], form of DNA methylation occurs
81 between the transcription start site and transcription end site of a gene, and is
82 known as gene body methylation (**GBM**) [27].
83 Previous studies have correlated GBM with stable and higher levels of
84 gene expression than genes without GBM [26, 28, 29, 30, 31], but its role in regulating
85 gene expression in specific developmental contexts such as the MZT is poorly
86 understood. Whole-genome bisulfite sequencing (WGBS) studies have shown
87 that DNA methylation patterns are dynamic during the MZT in vertebrate model
88 systems [32, 33, 34]. However, such methylation studies in vertebrates have focused
89 on cis-regulatory regions, including CpG islands in promoters and intergenic
90 regions. Disruption of methylation at CpG islands often has profound phenotypic
91 effects, while the role of GBM is less well understood. Because manipulating

92 DNA methylation machinery in vertebrate models affects both CpG islands and
93 GBM, it is difficult to identify functions of GBM that are independent of CpG
94 island methylation.

95 In contrast to vertebrates, DNA methylation occurs almost exclusively at
96 gene bodies in insects that have retained DNA methyltransferases 1 and 3
97 (DNMT1 and DNMT3) [19, 22, 35, 36]. Thus, such insect model systems have the
98 potential to make significant contributions in understanding the role of GBM in
99 development. A particularly attractive system with a full methylation toolkit and
100 exclusively gene body methylation is the wasp *Nasonia vitripennis* [36, 37, 38].

101 There are three DNMT1 paralogs in the *N. vitripennis* genome, and one of
102 them, *Nv-DNA methyltransferase 1a* (*Nv-Dnmt1a*)), was shown to be essential
103 for embryogenesis (the other two showed no obvious phenotype)[39]. Therefore, *N.*
104 *vitripennis* offers an exciting opportunity to functionally study the specific role of
105 gene body methylation in a well-defined developmental system. In this work, we
106 set out to experimentally investigate the role of *Nv-Dnmt1a* and thus identify a
107 role for gene body methylation in early embryogenesis of *N. vitripennis*.

108 Our detailed analysis of the developmental effects of *Nv-Dnmt1a* revealed
109 major defects in cellularization and morphogenesis of the early embryo, which
110 are phenotypes typically seen after disruption of the MZT in insects. Using
111 parental RNAi (pRNAi) and WGBS we found that the vast majority of gene body
112 methylation is lost when *Nv-Dnmt1a* is knocked down. We then show that loss of
113 gene body methylation during zygotic genome activation is correlated with
114 reduced gene expression from the affected locus during zygotic genome

115 activation. Furthermore, we found that genes that are not methylated, but whose
116 expression changed after *Nv-Dnmt1a* knockdown, were primarily upregulated in
117 knockdown embryos relative to control. *Nv-Dnmt1a* knockdown profoundly
118 altered the levels of expression of thousands of genes in the early embryo.
119

120 **Results**

121 ***Nv-Dnmt1a function is required for early embryonic events that require***
122 ***proper regulation of the zygotic genome***

123 The initial characterization of *Nv-Dnmt1a* showed that knockdown through
124 parental RNAi (pRNAi), where female embryos are injected with dsRNA [40], led to
125 lethality of embryos produced by injected females [39]. Understanding the precise
126 developmental failure(s) that lead to embryonic lethality should provide insight
127 into the functional importance of *Nv-Dnmt1a* for early embryonic development.
128 Therefore, we examined the embryonic development following *Nv-Dnmt1a*
129 pRNAi in more detail.

130 We first characterized the events of the first half of embryogenesis (0-15
131 hours, from egg lay to the completion of gastrulation) using time lapse imaging of
132 *Nv-Dnmt1a* pRNAi embryos. Similar to *D. melanogaster*, early development is
133 very rapid in *N. vitripennis.* During early embryogenesis, nuclei divide rapidly,
134 simultaneously, and without the formation of cell membranes to fill the large,
135 unicellular egg with syncytial nuclei. After 7 mitotic division cycles, nuclei migrate
136 to the cortex of the embryo, forming a syncytial blastoderm [41], consisting of a
137 single layer of nuclei populating the entire cortex of the egg. We observed no

138 obvious differences between control embryos and *Nv-Dnmt1a* pRNAi embryos
139 during the first 11 syncytial divisions. Syncytial blastoderm formation was
140 normal, and the last 4 divisions showed the characteristic increase in length
141 relative to earlier, pre blastoderm, cycles (Figure 1A).

142 The first obvious defect occurred at the 12th division cycle (Figure 1B, 1D).
143 There is normally a significant pause at this stage, as the nuclei are surrounded
144 by plasma membrane and thus transition from a syncytial to a cellular state, a
145 process referred to as cellularization (Figure 1A). Normally, cellularization
146 directly precedes the first morphogenetic movements of the embryo (gastrulation
147 and migration of the extraembryonic serosa) [41]. In this work, control embryos
148 began gastrulation 193 minutes after the onset of nuclear cycle 12, on average
149 (n=5, SD = 13.12, (Figure 1A)), similar to our previously published results in
150 untreated embryos [42]. Apparent morphogenetic movements in *Nv-Dnmt1a* pRNAi
151 embryos began significantly earlier, on average, 171 minutes (n=5, SD = 5.98)
152 into cycle 12 (Figure 1A).

153 In addition to being premature, these movements were abnormal. In *Nv-*
154 *Dnmt1a* pRNAi embryos, a line of cells at the anterior end of the embryo began
155 to ingress posteriorly (Figure 1D) which was not seen in control embryos (Figure
156 1B). In addition, internalization of the mesoderm and migration of the serosa from
157 the dorsal pole to cover the embryo both failed (Figure 1C, 1E).

158 To get a more detailed understanding of the cellular basis of these
159 defects, we examined high-resolution images of fixed and stained embryos at the
160 end of cycle 12 in control and knockdown samples. We imaged transverse

161 sections across the anterior-posterior axis of *Nv-Dnmt1a* pRNAi and control
162 embryos at the end of the 12th cell cycle, when the cellularization and the first
163 gastrulation movements should be occurring. Gastrulation in *N. vitripennis* is
164 different from what is seen in *D. melanogaster*. *N. vitripennis* embryos lack a
165 ventral furrow. Rather, the presumptive mesoderm on the ventral side of the
166 embryo forms a stiff plate. Subsequently, ectodermal cells separate from the
167 mesoderm at the lateral borders between the germ layers and crawl over this
168 mesodermal 'plate' before fusing over the mesoderm at the ventral midline [41].
169 During mid-cellularization, we observed membrane ingressing evenly
170 around each nucleus (Figure 2A) in control embryos. In contrast, membrane
171 ingression was uneven and did not wholly encapsulate nuclei in *Nv-Dnmt1a*
172 pRNAi embryos, leaving many nuclei completely or mostly uncovered prior to the
173 onset gastrulation (Figure 2C, white arrows point to examples of uncellularized
174 nuclei).
175 At the onset of morphogenesis, cell membranes fully enveloped each
176 blastoderm nucleus in control embryos, and a strong cable of actin was present
177 along the interior (basal) surface of the cellular blastoderm (Figure 2B-B', orange
178 arrowhead in 2B' marks the basal actin cable). Enlarged, round serosal cells
179 were present on the dorsal side, and the distinct population of presumptive
180 mesodermal cells was present on the ventral side (Figure 2C, pink arrowheads
181 mark the borders of the presumptive mesoderm), 24 out of 24 control embryos
182 are fully cellularized). In contrast, *Nv-Dnmt1a* pRNAi embryos lacked the cable of
183 actin along the interior surface of the blastoderm (Figure 2D-2D', orange

184 arrowhead marks uncellularized nuclei and obvious absence of the basal actin
185 cable), consistent with failed cellularization (23 out of 24 pRNAi embryos were
186 incompletely cellularized). In addition, the blastoderm was multilayered at many
187 locations, and clearly distinct serosal and mesodermal precursors were not
188 observed (Figure 2D).
189
190 ***Nv-Dnmt1a is required for global gene body methylation***
191 The failure of cellularization and morphogenesis are widely conserved
192 indicators of disrupted MZT [48, 53, 71]. Consequently, we hypothesized that
193 strong reduction of *Nv-Dnmt1a* by pRNAi would disrupt DNA methylation and
194 dysregulate zygotic genome activation in the early embryo of *N. vitripennis*. We
195 thus sought to characterize the DNA methylation patterns in the early embryo of
196 *N. vitripennis* and to examine how this pattern was affected when *Nv-Dnmt1a*
197 was depleted by pRNAi.
198 In control embryos (derived from mock-injected females) collected at the
199 late blastoderm stage (7-9 hours after egg-lay, corresponding to the time where
200 the developmental defects become evident) we identified 151,480 methylated
201 CpGs (mCGs) in a union set representing all of the different mCGs across three
202 biological replicates. Each sample contained very similar numbers of mCGs
203 across the three biological replicates (ranging from 136,410 to 136,717). The
204 vast majority of these mCGs were found within gene bodies (Table 1).
205 Mean fractional DNA methylation of gene bodies followed the canonical
206 bimodal distribution (Figure 3A) as seen in other invertebrate species including

207 insects [28]. Following the criteria used in a previous study we designated genes
208 with gene body fractional methylation levels of at least 0.02 as methylated genes
209 [27]. By this criterion we found 5423 methylated genes in the blastoderm embryo.
210 This is fewer than the 6008 methylated genes identified in adult *N. vitripennis*
211 tissues [36], where a slightly different method to define methylated genes was
212 used. This difference was to some degree, but not entirely, due to the methods
213 used because when we used the method described in [36], the number of
214 methylated genes identified in our samples increased to 5,685. Regardless of the
215 methods, 99% of the genes we designated as "methylated" in the blastoderm
216 embryo were also identified as methylated genes in adult wasps [36]. This
217 indicates that our results are highly compatible with those of Wang et al., 2013 [36],
218 and are consistent with the idea that GBM patterns are generally stable across
219 life stages.

220 We knocked-down *Nv-Dnmt1a* mRNA levels with pRNAi and examined
221 DNA methylation at the same developmental stage (7-9 hours after egg lay) as
222 the control. Based on our RNAseq results, *Nv-Dnmt1a* mRNA levels were
223 reduced by 5-fold in late blastoderm pRNAi samples relative to late blastoderm
224 control samples [43]. We observed a significant reduction in DNA methylation at
225 99.7% of methylated CpGs in the genome in pRNAi embryos. The magnitude of
226 the reduction was substantial, as we found an average of 81.5% DNA
227 methylation depletion per mCG (Figure 3B, 3C and Table 1).

228 While DNA methylation was strongly reduced genome-wide, the intragenic
229 pattern of GBM was maintained. For example, mCGs were enriched in exons

230 and were more numerous at the 5' end of the coding region of gene bodies in
231 control embryos (Figure 3D) similar to patterns found in other insects and other
232 developmental stages [23, 35, 44]. This pattern was maintained in pRNAi embryos,
233 despite the drastic overall reduction in DNA methylation levels (Figure 3D). This
234 suggests that *Nv-Dnmt1a* is required for gene body methylation but does not
235 govern the 5' and exon-biased pattern of DNA methylation that we see in
236 *Nasonia* and other hymenopteran insects.
237
238 ***Loss of Nv-Dnmt1a function disrupts the regulation of a large proportion of***
239 ***the early embryonic transcriptome***
240 Given the profound effects of *Nv-Dnmt1a* on global DNA methylation and
241 early developmental events, we sought to understand the effects of *Nv-Dnmt1a*
242 knockdown on gene expression over time in the early embryo. Although the
243 developmental effects *Nv-Dnmt1a* pRNAi were not visible until cellularization and
244 the onset of morphogenesis, we hypothesized that changes in the transcriptome
245 in response to disrupted development would occur earlier in development,
246 leading up to the multifaceted failure of development at gastrulation.
247 To test this, we performed RNA-seq on timed egg collections from mock
248 injected (control) and *Nv-Dnmt1a* dsRNA injected wasps at time points that cover
249 early embryogenesis from egg laying to gastrulation. The collection time points
250 were: freshly laid eggs (0-2 hours after egg lay), early blastoderm (3-5 hours after
251 egg lay), middle blastoderm (5-7 hours after egg lay) and late blastoderm/onset

252 of gastrulation (7-9 hours after egg lay, when the corresponding WGBS data
253 were collected).
254 We observed that there is a massive increase in the number of genes
255 significantly affected by *Nv-Dnmt1a* pRNAi the middle blastoderm stage that is
256 maintained into the late blastoderm (Fig 4A). We found 835 and 888 differentially
257 expressed genes (DEGs) in the egg and early blastoderm stages, respectively,
258 while there were 2744 and 1831 DEGs in the middle and late blastoderm stages,
259 respectively. The middle blastoderm stage corresponds to the most active part of
260 the MZT, where maternal mRNAs are being finally cleared and new transcription
261 from the zygotic genome becomes the predominant source of mRNAs.
262 Another intriguing pattern that appeared at the mid blastoderm stage is a
263 clear correlation between the direction of change of a DEG, and whether the
264 gene was methylated at the late blastoderm stage. Specifically, down-regulated
265 transcripts in *Nv-Dnmt1a* pRNAi middle blastoderm samples were largely derived
266 from methylated genes (1201 out of 1331 (90%)), while upregulated transcripts
267 came from non-methylated genes (1227/1413, 87%) (Figure 4A). Both of these
268 observations were statistically significant (Fisher's exact test, $P < 0.001$). A
269 nearly identical pattern was maintained into the late blastoderm stage (Fig. 4A,
270 B).
271 The strong correlation of methylated genes with down-regulation after *Nv-*
272 *Dnmt1a* pRNAi fits well with previous observations that methylated genes are
273 more highly and stably expressed than non-methylated genes in insects [19, 36, 45].
274 Furthermore, we have found that the magnitude of the reduction in expression

275 was highly correlated with the degree of lost methylation after pRNAi (Fig. 4C,
276 Pearson's correlation coefficient = 0.27, $P < 0.001$). This observation argues
277 strongly that gene expression changes of these genes are primarily a direct
278 effect of the loss of GBM.
279
280 ***Large-scale patterns of change differ between methylated and***
281 ***unmethylated differentially expressed genes***
282 Due to the chaotic and variable nature of the failures of cellularization and
283 morphogenesis, we hypothesized that the lethal phenotype is due to cascading
284 effects initiated by direct effects of *Nv-Dnmt1a* pRNAi on methylated genes which
285 could be amplified by downstream effects on unmethylated genes. The strong
286 correlation of DNA methylation state with the direction of expression level change
287 (Figure 2C) is consistent with this hypothesis and indicates that there are
288 fundamental differences in how these classes of genes are regulated in the early
289 embryo. Thus, we further examined variation of gene expression among genes
290 that showed differential expression between control and *Nv-Dnmt1a* pRNAi
291 treatments in at least one stage (a total of 3904 genes).
292 We identified 1769 methylated differentially expressed genes (mDEGs),
293 which showed a remarkably stable pattern of expression across all stages,
294 consistent with our understanding of methylated genes in general [31, 36]. Most
295 mDEGs were clustered at relatively high expression levels, with the frequency of
296 higher and lower expressed genes tapering rapidly and smoothly from this
297 cluster. While the general shape of the distribution was maintained after pRNAi,

298 the average expression was shifted significantly downward, particularly during
299 the middle and late blastoderm stages (Figure 5).
300 We identified 2135 unmethylated DEGs (uDEGs), which in comparison to
301 mDEGs, had a lower median expression (Figure 5). The concentration of gene
302 expression levels around the median is less pronounced. Most noticeably, there
303 was a significant proportion of uDEGs that were expressed at very low levels,
304 while such low expression levels were almost absent in the mDEGs.
305 *Nv-Dnmt1a* pRNAi had little effect on global distribution of uDEG
306 expression levels in the egg and early blastoderm stages (Figure 5A, B),
307 consistent with the minor effects of pRNAi on these stages reported earlier
308 (Figure 4A). However, in the middle and late blastoderm stages (Figure 5C, D),
309 we observed that very few genes were expressed at the very low levels. This
310 indicates that uDEGs that were absent or expressed at very low levels in control
311 were present at significantly higher levels after *Nv-Dnmt1a* pRNAi.
312 Formally, there are two explanations for this pattern, which are not
313 mutually exclusive. Increased mRNA from a given gene could be due to excess
314 transcription from the locus. Alternatively, higher levels at a given time point
315 could be due to a disruption in degradation of mRNA from a previous stage,
316 leading to the presence of excess reads.
317 To identify potentially informative subsets of DEGs, that were not obvious
318 from the global comparisons above, we used hierarchical clustering to group
319 genes based on the similarity of their patterns of expression over time in control
320 embryos and maintained the order of genes in *Nv-Dnmt1a* pRNAi embryos to

321 facilitate direct comparisons. Gene expression levels at different time points and
322 treatments were then plotted according to these clusters (Figure 6A,B).
323 Among all the mDEGs identified across the four timepoints, we identified a
324 cluster of transcripts that show upregulation in the early blastoderm *Nv-Dnmt1a*
325 pRNAi embryos relative to control embryos (Fig. 6A, blue box, dotted lines). The
326 genes in this cluster were provided maternally at very high expression levels
327 (median log2 expression value of 10) in both control and pRNAi samples (Figure
328 6C). In control embryos, expression levels fell precipitously for these genes as
329 development progressed (median log2 expression value of 7, an 8-fold reduction
330 from control (Figure 6C)).
331 In *Nv-Dnmt1a* pRNAi embryos, the levels of this set of genes also fall
332 significantly from egg to early embryo, but the magnitude of reduction is smaller
333 (median log2 expression value of ~8, a 4-fold reduction in median level), leading
334 to the appearance of upregulation relative to control at this stage (Figure 6C).
335 Thus, it appears that mRNA degradation downstream of Nv-Dnmt1a function
336 plays an important role in regulating levels maternally expressed, methylated
337 genes.
338 Among the uDEGs, we identified two clusters of interest. The larger of
339 these (Figure 6B, see black box) show much higher expression in middle and
340 late blastoderm in *Nv-Dnmt1a* pRNAi embryos relative to control. Expression
341 levels of these uDEGs are at low to moderate levels in eggs and early
342 blastoderm embryos in both control and pRNAi and remain so in the later stages
343 of control embryos (Figure 6B, compare consistent "cool" colors as opposed to

344 increased warmth in the RNAi samples). When we plot genes corresponding to
345 this cluster (change less than 2-fold between early and middle blastoderm
346 control, and are significantly higher after pRNAi in the middle blastoderm), we
347 found that 437 genes are mostly expressed at very low levels in the early
348 blastoderm in both control and pRNAi. At the middle blastoderm stage, there is a
349 significant general increase of these genes in the pRNAi case, while they remain
350 mostly unchanged at low levels in the control (Figure 6D). The most like
351 explanation for this pattern is that the increased levels in pRNAi embryos are due
352 to improper activation of these genes at the middle and late blastoderm stage.
353 There is another cluster of uDEGs whose relative levels in control
354 embryos increase markedly in the early blastoderm stage and then fall steeply in
355 the subsequent stages (Figure 6B, see red box). In *Nv-Dnmt1a* pRNAi embryos,
356 the initial increase is not affected, but levels do not fall as significantly at later
357 stages, leading to an apparent upregulation of their transcripts relative to control
358 embryos in later stages (Figure 6B). The 615 genes that fit this profile show
359 again very similar distributions between the control and pRNAi cases in the early
360 blastoderm. In contrast there is a severe drop in levels for the control embryos at
361 the middle blastoderm stage, while the pRNAi levels decrease less dramatically
362 (Supplemental figure 1). This pattern is similar for the 376 mDEGs that were
363 apparently upregulated in the early blastoderm stage (Figure 6A,C) and indicates
364 that regulation of mRNA degradation is affected downstream of *Nv-Dnmt1a*
365 pRNAi during the major phase of the MZT.
366

367 ***Many potential targets for mediating the developmental effects of Nv-***
368 ***Dnmt1a pRNAi***

369 While there is no single obvious candidate gene to explain our results,
370 there are many RNA binding and regulating factors, as well as transcription
371 factors, cyclins and cytoskeletal components that could plausibly play important
372 roles in producing the patterns of gene expression change and developmental
373 failure after pRNAi. We performed gene ontology analyses, and found that terms
374 involved in metabolism, and other basal cell functions were the most significantly
375 and consistently enriched in both in methylated and unmethylated DEGs
376 throughout development (Suppl. Table 1). In addition, we found that RNA
377 degradation is an enriched category of methylated genes, which could explain
378 part of the pattern of gene expression change (Suppl. Table 1).

379 Among the RNA binding factors affected by *Nv-Dnmt1a* pRNAi are
380 homologs of the well-known MZT factors *Smaug* and the CCR-NOT deadenlyase
381 complex. Fascinatingly, we also found that an ortholog of the *D. melanogaster*
382 nonsense mediated mRNA decay (NMD) component *nonC (Nv-nonC)* was down-
383 regulated after *Nv-Dnmt1a* pRNAi. While the *D. melanogaster* gene has no role
384 in embryogenesis [46], the mouse ortholog (named Smg1 after the *C. elegans*
385 gene (no relation to *smaug*), which is the founding member of this gene family [47])
386 is required for embryogenesis [48]. Furthermore, the human ortholog of
387 *Smg1*/*nonC* is regulated by DNA methylation in humans [49]. We decided to
388 functionally test whether *Nv-nonC* could be an important intermediary in

389 producing the defects in cellularization and gastrulation when *Nv-Dnmt1a* was
390 knocked down.
391 Live imaging of *Nv-nonC* knock-down embryos revealed that affected
392 embryos consistently arrested at nuclear cycle 11 and did not proceed to the final
393 syncytial division or gastrulation (Supplemental Movie 1). This is more severe
394 than the strongest *Nv-Dnmt1a* phenotypes, so we cannot say for certain the
395 exact role of *Nv-nonC* in the regulatory networks downstream of *Nv-Dnmt1a* at
396 the moment. However, the phenotype is consistent with *Nv-Smg1* having an
397 important role in the transition from egg to embryo, and its partial reduction and
398 disturbance of its potential interaction partners after *Nv-Dnmt1a* pRNAi might
399 play a significant role in the failures of cellularization and gastrulation.
400
401 **Discussion**
402 A previous study found that one of the DNMT1 orthologs in the wasp (*Nv-*
403 *Dnmt1a*) was required for *Nasonia* embryogenesis, while the other two DNMT1
404 paralogs (*Nv-Dnmt1b*, *Nv-Dnmt1c*) and the DNMT3 ortholog *Nv-dnmt3* were
405 apparently dispensable [39]. *Nv-Dnmt1a* pRNAi embryos failed to form segments
406 and the knockdown was lethal [39] which led us to further examine the phenotype
407 in more detail [50, 51].
408 We found that the first signs of developmental failure are nuclei that fail to
409 be correctly cellularized. This directly precedes failure of the morphogenetic
410 processes of mesoderm internalization, and migration of the serosa. These are
411 all developmental events that are strongly affected when the MZT is disrupted in

412 *N. vitripennis* and *D. melanogaster*. Consistent with this, *Nv-Dnmt1a* knockdown
413 was associated with major disruption of gene expression levels during early
414 embryogenesis. The most significant alterations to the transcriptome occurred at
415 the mid blastoderm stage, which correlates well with when the major wave of
416 zygotic genome activation occurs in *N. vitripennis*. This observation, in
417 combination with our finding that GBM was significantly reduced after *Nv-Dnmt1a*
418 pRNAi, strongly indicates that loss of gene body methylation disrupts the MZT in
419 *N. vitripennis*.
420 The exact mechanism by which Nv-Dnmt1a regulates the MZT and
421 downstream processes is not yet understood. However, our current results
422 provide a good basis to generate hypotheses. A crucial observation was that
423 there was an extremely strong correlation between methylation state of a gene
424 and the direction of expression change after *Nv-Dnmt1a* pRNAi: downregulated
425 genes in pRNAi embryos were almost all methylated in control embryos, and
426 upregulated genes were conversely almost exclusively unmethylated (Figure 4).
427 Previous studies posited that gene body methylation has an important role
428 in facilitating high, steady levels of gene expression [17, 36]. However, whether gene
429 body methylation directly regulates levels of gene expression has been
430 controversial [52, 53]. Phylogenetic analyses of methylated and unmethylated plant
431 species as well as analyses of within-species variation of gene body methylation
432 in plants [52, 53, 54] led to at most weak effects of gene body methylation on gene
433 expression, although the evolutionary conservation of gene body methylation
434 indicated associated functionality. Here we show that as a result of pRNAi of *Nv-*

435 *Dnmt1a*, nearly all methylated genes show dramatic reduction of gene
436 expression. Moreover, the degree of expression reduction directly correlated with
437 the degree of gene body methylation loss. As far as we are aware, these are the
438 first such demonstrations directly linking gene body DNA methylation to gene
439 expression levels.

440 Another novel finding is that nearly all of the unmethylated differentially
441 expressed genes were upregulated in *Nv-Dnmt1a* pRNAi relative to control.
442 Presumably the effects of *Nv-Dnmt1a* pRNAi on unmethylated genes are indirect
443 and are more proximally caused by the disrupted expression of the methylated
444 genes. It is not clear why such indirect effects result in such a large bias toward
445 increased gene expression.

446 Our results point to the middle blastoderm stage as the crucial point where
447 *Nv-Dnmt1a* has its strongest effects on the embryonic transcriptome. Our data
448 also show that the indirect effects of *Nv-Dnmt1a* pRNAi are mediated by both
449 disruption of mRNA degradation, and misregulation of transcription from the
450 zygotic genome. Thus, *Nv-Dnmt1a* appears to exert its strongest effects at the
451 time, and using the molecular processes, that are most characteristic of the MZT.
452 We therefore propose that GBM is a crucial component of the MZT in *Nasonia*,
453 and that this epigenetic mark is likely to play an important role in the MZT in other
454 insects.

455

456 **Methods**

457 <u>Live imaging</u>

458 All embryos were live-imaged as described in Arsala & Lynch 2017. Briefly, we
459 live-imaged all embryos at 28C for 15 hours on an Olympus BX-80 inverted
460 microscope under 30X silicone immersion and DIC optics.
461
462 Embryo Collection
463 All embryos used for fluorescence in situ hybridizations were collected and fixed
464 as described as in Buchta et al., 2013 [41].
465
466 Ovary Collection
467 Mothers were cold anesthetized and their ovaries were hand-dissected and
468 extracted using stainless-steel needles. The ovaries were fixed in 5%
469 formaldehyde for 30 minutes and subsequently used for fluorescence in-situ
470 hybridization.
471
472 Phalloidin staining & transverse sectioning
473 Control injected and *Nv-Dnmt1a* dsRNA (1ug/ul) injected mothers were allowed
474 to lay eggs on hosts for 2 hours at 25C. Freshly laid eggs were collected from
475 hosts and aged on 1% agarose PBS plates at 25C until they were 8-10 hours old,
476 so that all embryos were aged to correspond with the onset of gastrulation. We
477 hand dissected the chorions of fixed embryos. Afterward, the fixed embryos
478 were placed in 1X PBS and stained with AlexaFluor 488 phalloidin at a 1:250
479 dilution. The stained, fixed embryos were placed in vectashield with DAPI
480 overnight. Finally, the embryos were laid flat on a cover slip and were cut in half

481 along the transverse axis using a razor slotted into an embryo ‘guillotine.’ The
482 resulting embryo ‘halves’ were flipped ‘up’ on the cover slip and imaged on an
483 Andor Revolution WD spinning disc confocal system. The samples were
484 illuminated with 488nm (phalloidin) and 405nm (DAPI) diode laser and Z-stack
485 images were captured using a 30x objective at 1micron increments.
486
487 RNA extraction
488 Embryos were collected and aged as described above. We designed 3 non-
489 overlapping dsRNA constructs and injected 100 females per biological replicate
490 with either 1µg/mL dsRNA diluted in water or with water as a control. The
491 females were left unmated, so that all resulting progeny were male as the
492 variation in sex and ploidy could confound our analysis. The injected females
493 were allowed to lay eggs that were aged at 25C until they reached the following
494 four time points across the MZT: 0-2hours to generate a freshly laid egg
495 transcriptome, 3-5hours to generate an early blastoderm transcriptome, 5-7
496 hours to generate a middle blastoderm transcriptome, 7-9 hours to generate late
497 blastoderm embryos that are at the onset of gastrulation. Once the embryos
498 reached the time points, we isolated 100ng of total RNA using TRI Reagent for
499 all samples in biological triplicate. We confirmed the RIN value for all samples
500 were above 9.0 using a 2100 Agilent Bioanalyzer and immediately prepared 24
501 libraries for sequencing.
502
503 RNA library preparation and bulk RNA-sequencing

504 Using the 100ng of total RNA from each sample isolated above, we performed
505 poly-A tail selection using the NEBNext Poly (A) mRNA magnetic isolation
506 module (E7490) and immediately proceeded with library preparation. Libraries
507 were prepared for bulk RNA-sequencing using the NEBNext Ultra Directional
508 RNA Library Prep Kit for Illumina (E7420). The libraries were purified, validated
509 and pooled before sequencing. The libraries were subjected to 100bp paired-end
510 sequencing across 2 lanes on a HiSeq4000.
511
512 RNA-seq analysis
513 To assess sequencing quality, we using FastQC and saw high quality reads
514 across all samples. We trimmed adapters and removed low quality reads using
515 Trim Galore-0.6.0 only using the --paired parameter. We reassessed the trimmed
516 read quality using FastQC and proceeded to map the reads to genome using
517 HISAT2-2.0.5 (hisat2 -p 8 --max-intronlen 10000 -q –x). Differential expression
518 analysis was performed using the R package DESeq2[55].
519
520 DNA extraction and bisulfite library preparation
521 We extracted and purified genomic DNA from embryos using the QIAamp DNA
522 Micro Kit (Qiagen 56304). 40ng of genomic DNA was bisulfite converted and
523 libraries were prepared at the University of Chicago Genomics Facility using the
524 Accel-NGS Methyl-Seq DNA Library Kit from Swift Biosciences.
525
526 Analysis of Bisulfite-sequencing data

527 CpG sites were determined to methylated using a binomial test [22, 36] where the
528 rate of deamination representing the probability of success and total number of
529 reads representing the number of trials [22, 36]. P-values were then corrected for
530 multiple testing [56] and CpGs with adjusted P-values of < 0.05 were labeled as
531 methylated CpGs. Genes containing at least one methylated CpG were
532 subsequently labeled as methylated genes. Fractional methylation of CpGs was
533 calculated by dividing the number of methylated reads by the total number of
534 reads and the fractional methylation of genes was calculated by taking the
535 average fractional methylation of all CpGs within the gene body.
536 For the differential methylation analysis, only CpG sites that were methylated in
537 at least one control sample were retained similar to previous insect studies [45, 57].
538 The DSS package [58] was used to assess differentially methylated CpGs with
539 RNAi status as the sole predictor of methylation. P-values for each CpG site was
540 adjusted for multiple testing [56] with significance level set at an adjusted P-value
541 of < 0.1. Genes with at least one differentially methylated CpG were considered
542 as differentially methylated genes.
543
544
545 **Figure Legends:**
546
547 **Figure 1.** Live imaging of control and *Nv-Dnmt1a* RNAi embryos. A-A') Live-
548 imaging of a control embryo at the onset of gastrulation and at post-gastrulation.
549 Peach arrows in (A) point to the initial mesodermal folds which are eventually

550 internalized by A'. The blue arrowhead in A' points to the serosa. Scale bars
551 (black lines in A-A') are 50μm. (B-B') Live-imaging of a *Nv-Dnmt1a* RNAi embryo
552 at the onset of gastrulation and at what is equivalent to post-gastrulation.
553 Defective mesodermal folds are denoted by peach arrowheads in B and B'.
554 Abnormal serosal movements are denoted by a blue arrowhead in B'. C) Box
555 and whisker plot displaying the length of blastoderm division times that were
556 measured during live imaging experiments. Nc = nuclear cycle #. P values were
557 determined by performing a 2-tailed T-test assuming unequal variance between
558 RNAi and control. N=5 control, N=5 *Nv-Dnmt1a* RNAi. All scale bars (black lines
559 in A-A') represent 50 μm.
560
561 **Figure 2.** Transverse views of control and *Nv-Dnmt1a* RNAi embryos during
562 cellularization and at the onset of gastrulation. Green, phalloidin (F-actin). white,
563 DAPI (DNA). (A) Control embryo during mid cellularization. (B) Control embryo at
564 the onset of gastrulation. Pink arrowheads demarcate the borders of the
565 presumptive mesoderm. (B') Zoomed in view of fully cellularized control embryo.
566 Orange arrowhead points to the basal actin cable. (C) *Nv-Dnmt1a* RNAi embryo
567 during mid-cellularization. White arrows point to examples of disordered nuclei.
568 (D) *Nv-Dnmt1a* RNAi embryo at the onset of gastrulation. White arrows point to
569 examples of uncellularized, disordered nuclei. (D') Zoomed in view of an *Nv-*
570 *Dnmt1a* RNAi embryo that fails to fully cellularize. Orange arrowhead points to an
571 uncellularized nucleus (note the absence of the basal actin cable). (E) Table with
572 n values of cellularized and incompletely cellularized control and *Nv-Dnmt1a*

573 RNAi embryos. *** = p value > 0.0001 determined by Fisher's Exact Test. All
574 scale bars (white lines in A-A''') represent 10 μm.
575
576 **Figure 3**. Global DNA methylation in control and *Nv-Dnmt1a* pRNAi late
577 blastoderm *N. vitripennis* embryos. (A) An example of distribution of fractional
578 DNA methylation in control embryo exhibiting the classical bimodal distribution.
579 We defined methylated genes as genes with a minimum of 0.02 gene body
580 methylation (shown as the dashed line) to classify methylated and unmethylated
581 genes. (B) DNA methylation is substantially reduced in *Nv-Dnmt1a* pRNAi
582 samples compared to the control samples. (C) Distributions of fractional
583 methylation of CpGs that are methylated at least one control sample demonstrate
584 that CpGs lose DNA methylation in RNAi embryos. (D) Distribution of mean
585 fractional methylation in the first and last four exons and introns of methylated
586 genes. Control samples shown in red, RNAi embryos shown in blue.
587
588 **Figure 4.** Gene expression of methylated and unmethylated genes in control and
589 *Nv-Dnmt1a* RNAi *N. vitripennis* embryos. **(**A) Volcano plots showing differentially
590 expressed genes between control and *Nv-Dnmt1a* RNAi in embryos of different
591 developmental stages. X axis is $\log_2$ fold change in *Nv-Dnmt1a* RNAi samples
592 relative to control samples. Y axis is $\log_{10}$ adjusted p-values. Golden dots are
593 methylated, significantly differentially expressed (FDR-corrected $P \leq 0.1$). Purple
594 dots are significant and DEGs that are unmethylated (FDR-corrected $P \leq 0.1$).
595 Blue and grey are non-significant and represent methylated and unmethylated

596 genes, respectively. (B) Distribution of methylated and unmethylated genes for all
597 genes in the genome, differentially methylated genes (DMGs), down-regulated
598 differentially expressed genes (Down DEGs), and up-regulated differentially
599 expressed genes (Up DEGs). (C) The correlation between relative GBM change
600 and relative expression change (calculated as $\log_2$-fold change) in the RNAi
601 samples compared to the control samples was positive and statistically
602 significant (Pearson R = 0.27, $P < 0.001$).
603
604 **Figure 5.** Violin plots of methylated and unmethylated differentially expressed
605 genes (DEGs) in control and *Nv-Dnmt1a* pRNAi eggs, early blastoderm embryos,
606 middle blastoderm embryos, and late blastoderm embryos.
607
608 **Figure 6.** Differentially expressed methylated and unmethylated gene expression
609 in *Nv-Dnmt1a* pRNAi and control *N. vitripennis* embryos. (A) Heatmap of 1769
610 methylated differentially expressed genes (mDEGs) and their expression over
611 time in control and *Nv-Dnmt1a* pRNAi samples represented as Z-scores. Blue
612 boxes on the heatmap highlight a cluster of mDEGs that are of interest and
613 discussed in the text. (B) Heatmap of 2135 unmethylated DEGs (uDEGs) and
614 their expression over time in control and *Nv-Dnmt1a* pRNAi samples represented
615 as Z-scores. Black and red boxes on the heatmap highlight two clusters of
616 uDEGs that are of interest and discussed in the text. (C) Violin plots of 376
617 mDEGs in *Nv-Dnmt1a* pRNAi eggs and early blastoderm embryos. These
618 mDEGs are significantly enriched in the early blastoderm *Nv-Dnmt1a* pRNAi

samples relative to control early blastoderm embryos. Both comparisons were subjected to a t-test. ns = not significant, *** P<0.001 by t-test.

(D) Violin plots of 213 uDEGs in control and *Nv-Dnmt1a* pRNAi early and middle blastoderm embryos (B). ns = not significant, *** P<0.001 by t-test.

References

1. Tadros W, Lipshitz HD. The maternal-to-zygotic transition: a play in two acts. *Development* **136**, 3033-3042 (2009).

2. Vastenhouw NL, Cao WX, Lipshitz HD. The maternal-to-zygotic transition revisited. *Development* **146**, dev161471 (2019).

3. Tadros W*, et al.* SMAUG is a major regulator of maternal mRNA destabilization in Drosophila and its translation is activated by the PAN GU kinase. *Developmental cell* **12**, 143-155 (2007).

4. Laver JD*, et al.* Brain tumor is a sequence-specific RNA-binding protein that directs maternal mRNA clearance during the Drosophila maternal-to-zygotic transition. *Genome biology* **16**, 94 (2015).

5. Fu S, Nien C-Y, Liang H-L, Rushlow C. Co-activation of microRNAs by Zelda is essential for early Drosophila development. *Development* **141**, 2108-2118 (2014).

6. Bushati N, Stark A, Brennecke J, Cohen SM. Temporal reciprocity of miRNAs and their targets during the maternal-to-zygotic transition in Drosophila. *Current Biology* **18**, 501-506 (2008).

7. Schulz KN*, et al.* Zelda is differentially required for chromatin accessibility, transcription factor binding, and gene expression in the early Drosophila embryo. *Genome research* **25**, 1715-1726 (2015).

8. Dahanukar A, Walker JA, Wharton RP. Smaug, a novel RNA-binding protein that operates a translational switch in Drosophila. *Molecular cell* **4**, 209-218 (1999).

657 9. Hamm DC, Harrison MM. Regulatory principles governing the maternal-to-
658 zygotic transition: insights from Drosophila melanogaster. *Open Biol* **8**,
659 (2018).
660
661 10. Urieli-Shoval S, Gruenbaum Y, Sedat J, Razin A. The absence of
662 detectable methylated bases in Drosophila melanogaster DNA. *FEBS*
663 *letters* **146**, 148-152 (1982).
664
665 11. Simpson VJ, Johnson TE, Hammen RF. Caenorhabditis elegans DNA
666 does not contain 5-methylcytosine at any time during development or
667 aging. *Nucleic acids research* **14**, 6711-6719 (1986).
668
669 12. Jiang N, Wang L, Chen J, Wang L, Leach L, Luo Z. Conserved and
670 Divergent Patterns of DNA Methylation in Higher Vertebrates. *Genome*
671 *Biology and Evolution* **6**, 2998-3014 (2014).
672
673 13. Deaton AM, Bird A. CpG islands and the regulation of transcription. *Genes*
674 *& development* **25**, 1010-1022 (2011).
675
676 14. Santos F, Hendrich B, Reik W, Dean W. Dynamic reprogramming of DNA
677 methylation in the early mouse embryo. *Developmental biology* **241**, 172-
678 182 (2002).
679
680 15. Yartseva V, Giraldez AJ. The Maternal-to-Zygotic Transition During
681 Vertebrate Development: A Model for Reprogramming. *Current topics in*
682 *developmental biology* **113**, 191-232 (2015).
683
684 16. Lyko F. The DNA methyltransferase family: a versatile toolkit for
685 epigenetic regulation. *Nature Reviews Genetics* **19**, 81 (2018).
686
687 17. Bewick AJ, Vogel KJ, Moore AJ, Schmitz RJ. Evolution of DNA
688 methylation across insects. *Molecular biology and evolution* **34**, 654-665
689 (2017).
690
691 18. Provataris P, Meusemann K, Niehuis O, Grath S, Misof B. Signatures of
692 DNA methylation across insects suggest reduced DNA methylation levels
693 in Holometabola. *Genome biology and evolution* **10**, 1185-1197 (2018).
694
695 19. Ventos-Alfonso A, Ylla G, Montanyes J-C, Belles X. DNA methylation in
696 cockroaches is essential in early embryo development and reduces gene
697 expression noise. *bioRxiv*, (2020).
698
699 20. Yi S. Birds do it, bees do it, worms and ciliates do it too: DNA methylation
700 from unexpected corners of the tree of life. *Genome biology* **13**, (2012).
701

21. Bonasio R*, et al.* Genome-wide and caste-specific DNA methylomes of the ants Camponotus floridanus and Harpegnathos saltator. *Current Biology* **22**, 1755-1764 (2012).

22. Lyko F, Foret S, Kucharski R, Wolf S, Falckenhayn C, Maleszka R. The honey bee epigenomes: differential methylation of brain DNA in queens and workers. *PLoS biology* **8**, (2010).

23. Walsh TK*, et al.* A functional DNA methylation system in the pea aphid, Acyrthosiphon pisum. *Insect Molecular Biology* **19**, 215-228 (2010).

24. Bird A. Functions for DNA methylation in vertebrates. In: *Cold Spring Harbor Symposia on Quantitative Biology*). Cold Spring Harbor Laboratory Press (1993).

25. Keller TE, Han P, Yi SV. Evolutionary Transition of Promoter and Gene Body DNA Methylation across Invertebrate–Vertebrate Boundary. *Molecular Biology and Evolution* **33**, 1019-1028 (2016).

26. Zemach A, McDaniel IE, Silva P, Zilberman D. Genome-wide evolutionary analysis of eukaryotic DNA methylation. *Science* **328**, 916-919 (2010).

27. Sarda S, Zeng J, Hunt BG, Yi SV. The evolution of invertebrate gene body methylation. *Molecular biology and evolution* **29**, 1907-1916 (2012).

28. Hellman A, Chess A. Gene body-specific methylation on the active X chromosome. *Science* **315**, 1141-1143 (2007).

29. Maunakea AK*, et al.* Conserved role of intragenic DNA methylation in regulating alternative promoters. *Nature* **466**, 253-257 (2010).

30. Hunt BG, Glastad KM, Yi SV, Goodisman MAD. The Function of Intragenic DNA Methylation: Insights from Insect Epigenomes. *Integr Comp Biol* **53**, 319-328 (2013).

31. Huh I, Zeng J, Park T, Yi SV. DNA methylation and transcriptional noise. *Epigenetics & Chromatin* **6**, (2013).

32. Smith ZD*, et al.* DNA methylation dynamics of the human preimplantation embryo. *Nature* **511**, 611-615 (2014).

33. Li L, Lu X, Dean J. The maternal to zygotic transition in mammals. *Molecular aspects of medicine* **34**, 919-938 (2013).

34. Guo H*, et al.* The DNA methylation landscape of human early embryos. *Nature* **511**, 606-610 (2014).

35. Bewick AJ, Sanchez Z, Mckinney EC, Moore AJ, Moore PJ, Schmitz RJ. Dnmt1 is essential for egg production and embryo viability in the large milkweed bug, Oncopeltus fasciatus. *Epigenetics & chromatin* **12**, 1-14 (2019).

36. Wang X*, et al.* Function and Evolution of DNA Methylation in Nasonia vitripennis. *PLoS Genetics* **9**, e1003872 (2013).

37. Park J*, et al.* Comparative analyses of DNA methylation and sequence evolution using Nasonia genomes. *Molecular biology and evolution* **28**, 3345-3354 (2011).

38. Werren JH, Richards S, Desjardins CA, Niehuis O, Gadau J, Colbourne JK. Functional and Evolutionary Insights from the Genomes of Three Parasitoid Nasonia Species. *Science* **327**, 343-348 (2010).

39. Zwier M, Verhulst E, Zwahlen R, Beukeboom L, Van de Zande L. DNA methylation plays a crucial role during early Nasonia development. *Insect molecular biology* **21**, 129-138 (2012).

40. Lynch JA, Desplan C. A method for parental RNA interference in the wasp Nasonia vitripennis. *Nat Protoc* **1**, 486-494 (2006).

41. Buchta T, Özüak O, Stappert D, Roth S, Lynch JA. Patterning the dorsal–ventral axis of the wasp Nasonia vitripennis. *Developmental biology* **381**, 189-202 (2013).

42. Arsala D, Lynch JA. Ploidy has little effect on timing early embryonic events in the haplo-diploid wasp Nasonia. *Genesis (New York, NY : 2000)* **55**, (2017).

43. Arsala D, Wu X, Yi SV, Lynch JA. Supplemental item 1.) (2020).

44. Wang Y*, et al.* Functional CpG methylation system in a social insect. *Science* **314**, 645-647 (2006).

45. Wu X, Lindsey AR, Chatterjee P, Werren JH, Stouthamer R, Soojin VY. Distinct epigenomic and transcriptomic modifications associated with Wolbachia-mediated asexuality. *PLoS pathogens* **16**, e1008397 (2020).

46. Chen Z, Smith KR, Batterham P, Robin C. Smg1 nonsense mutations do not abolish nonsense-mediated mRNA decay in Drosophila melanogaster. *Genetics* **171**, 403-406 (2005).

47. Pulak R, Anderson P. mRNA surveillance by the Caenorhabditis elegans smg genes. *Genes & development* **7**, 1885-1897 (1993).

48. McIlwain DR*, et al.* Smg1 is required for embryogenesis and regulates diverse genes via alternative splicing coupled to nonsense-mediated mRNA decay. *Proceedings of the National Academy of Sciences* **107**, 12186-12191 (2010).

49. Bhuvanagiri M*, et al.* 5-azacytidine inhibits nonsense-mediated decay in a MYC-dependent fashion. *EMBO molecular medicine* **6**, 1593-1609 (2014).

50. Eckersley-Maslin MA, Alda-Catalinas C, Reik W. Dynamics of the epigenetic landscape during the maternal-to-zygotic transition. *Nature Reviews Molecular Cell Biology* **19**, 436-450 (2018).

51. Dunican DS, Ruzov A, Hackett JA, Meehan RR. xDnmt1 regulates transcriptional silencing in pre-MBT Xenopus embryos independently of its catalytic function. *Development* **135**, 1295-1302 (2008).

52. Seymour DK, Gaut BS. Phylogenetic Shifts in Gene Body Methylation Correlate with Gene Expression and Reflect Trait Conservation. *Molecular Biology and Evolution* **37**, 31-43 (2020).

53. Bewick AJ, Zhang YW, Wendte JM, Zhang XY, Schmitz RJ. Evolutionary and Experimental Loss of Gene Body Methylation and Its Consequence to Gene Expression. *G3-Genes Genom Genet* **9**, 2441-2445 (2019).

54. Takuno S, Seymour DK, Gaut BS. The Evolutionary Dynamics of Orthologs That Shift in Gene Body Methylation between Arabidopsis Species. *Molecular Biology and Evolution* **34**, 1479-1491 (2017).

55. Love MI, Huber W, Anders S. Moderated estimation of fold change and dispersion for RNA-seq data with DESeq2. *Genome biology* **15**, 550 (2014).

56. Benjamini Y, Hochberg Y. Controlling the false discovery rate: a practical and powerful approach to multiple testing. *Journal of the Royal statistical society: series B (Methodological)* **57**, 289-300 (1995).

57. Hu H*, et al.* In-depth proteome of the hypopharyngeal glands of honeybee workers reveals highly activated protein and energy metabolism in priming the secretion of royal jelly. *Molecular & Cellular Proteomics* **18**, 606-621 (2019).

58. Park Y, Wu H. Differential methylation analysis for BS-seq data under general experimental design. *Bioinformatics* **32**, 1446-1453 (2016).

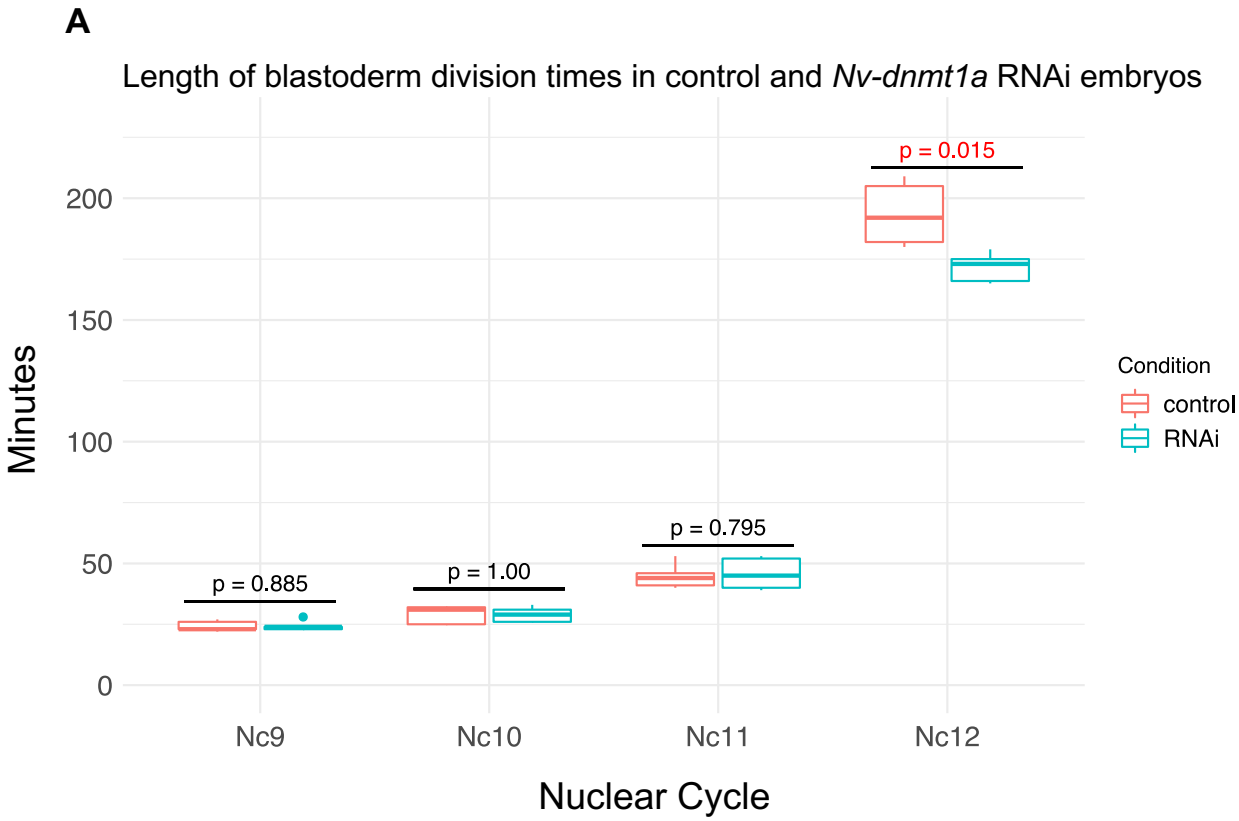
A
Length of blastoderm division times in control and *Nv-dnmt1a* RNAi embryos
Minutes
200
150
100
50
0
p = 0.885
p = 1.00
p = 0.795
p = 0.015
Nc9
Nc10
Nc11
Nc12
Nuclear Cycle
Condition
control
RNAi

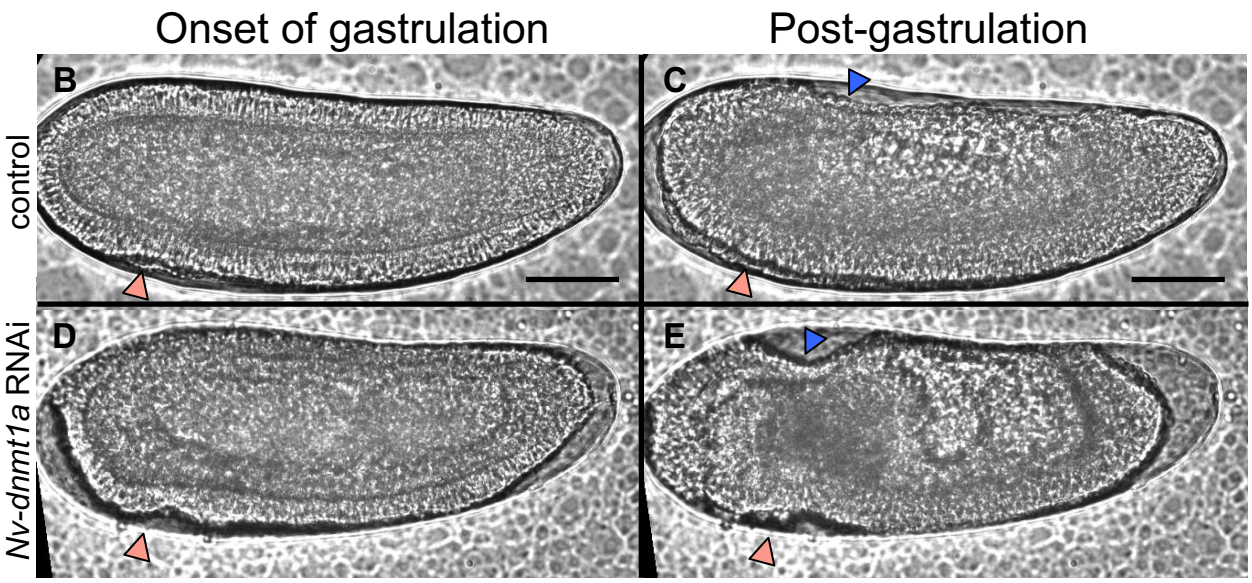
Onset of gastrulation
Post-gastrulation
control
Nv-dnmt1a RNAi
B
C
D
E

Figure 2

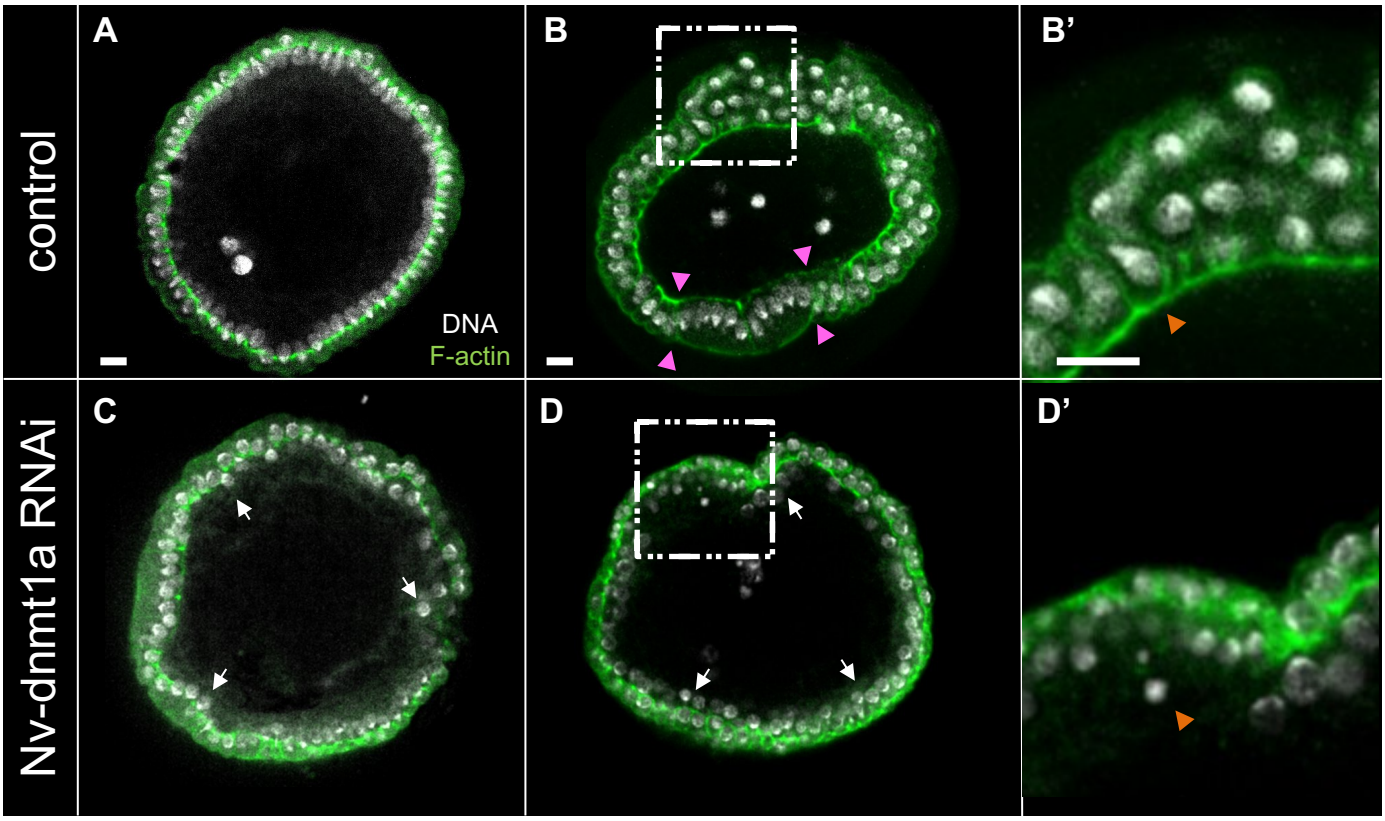

E

Condition	Cellularized	Incomplete Cellularization
Control	24	0
Nv-dnmt1a RNAi	1	23***

Table 1

Sample	Non-conversion rate	Median CpG coverage	Mean CpG coverage	Methylated CpGs (mCGs)	mCGs within gene bodies
Control 1	0.0052	14	14.92	136,600	126,333
Control 2	0.0051	15	15.63	136,410	126,174
Control 3	0.0055	14	14.75	136,717	126,364
RNAi 1	0.0052	14	14.30	98,511	91,874
RNAi 2	0.0051	14	14.48	8,017	7,720
RNAi 3	0.0053	14	14.91	15,305	14,669

Table 1. Summary CpG statistics and non-conversion rates for each sample.

Figure 3

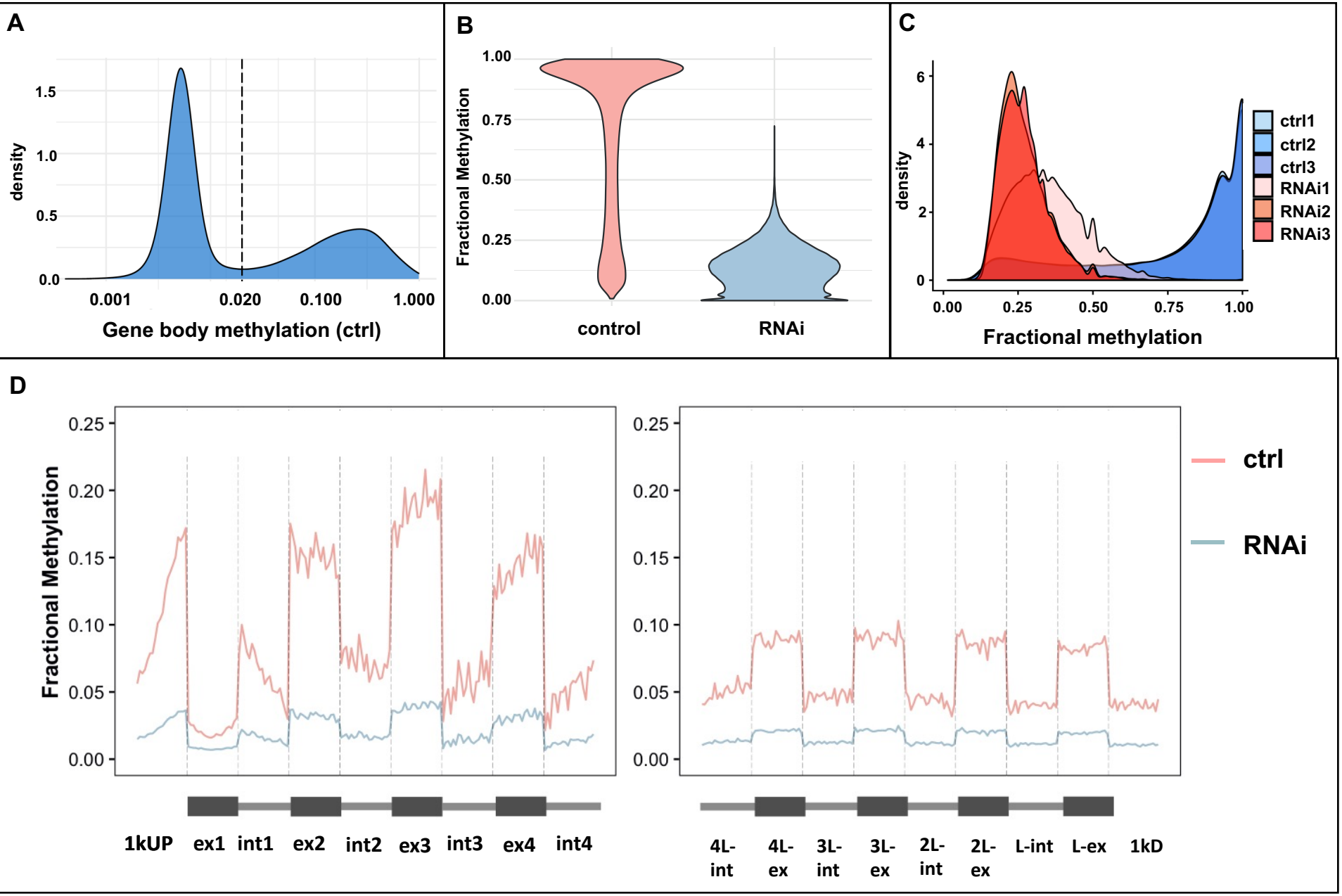
A
density
1.5
1.0
0.5
0.0
0.001
0.020
0.100
1.000
Gene body methylation (ctrl)
B
Fractional Methylation
1.00
0.75
0.50
0.25
0.00
control
RNAi
C
density
6
4
2
0
0.00
0.25
0.50
0.75
1.00
Fractional methylation
ctrl1
ctrl2
ctrl3
RNAi1
RNAi2
RNAi3
D
Fractional Methylation
0.25
0.20
0.15
0.10
0.05
0.00
1kUP
ex1
int1
ex2
int2
ex3
int3
ex4
int4
4L-int
4L-ex
3L-int
3L-ex
2L-int
2L-ex
L-int
L-ex
1kD
ctrl
RNAi

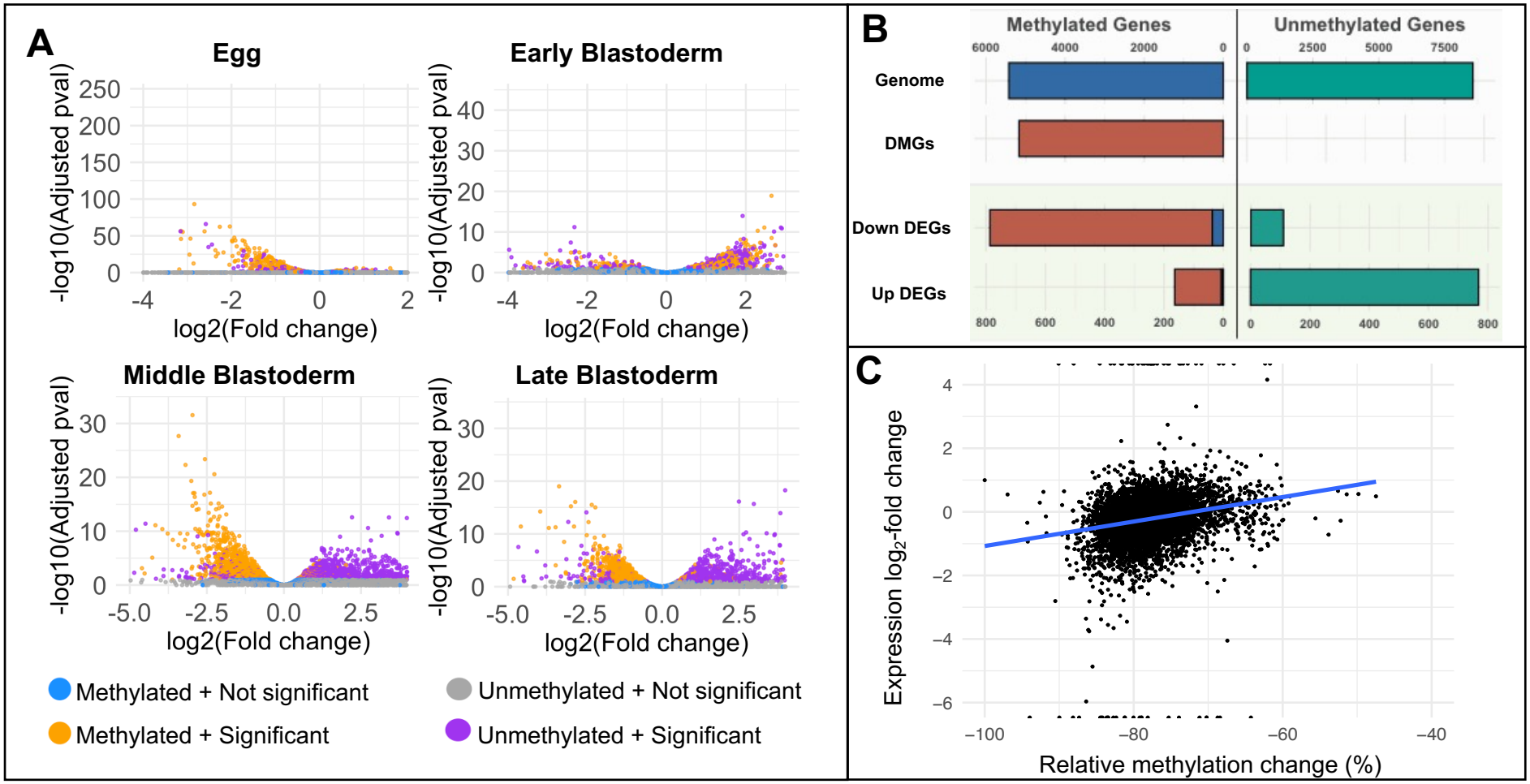
A
Egg
Early Blastoderm
Middle Blastoderm
Late Blastoderm
-log10(Adjusted pval)
log2(Fold change)
Methylated + Not significant
Methylated + Significant
Unmethylated + Not significant
Unmethylated + Significant
B
Methylated Genes
Unmethylated Genes
Genome
DMGs
Down DEGs
Up DEGs
C
Expression log2-fold change
Relative methylation change (%)

Figure 4

Figure 5

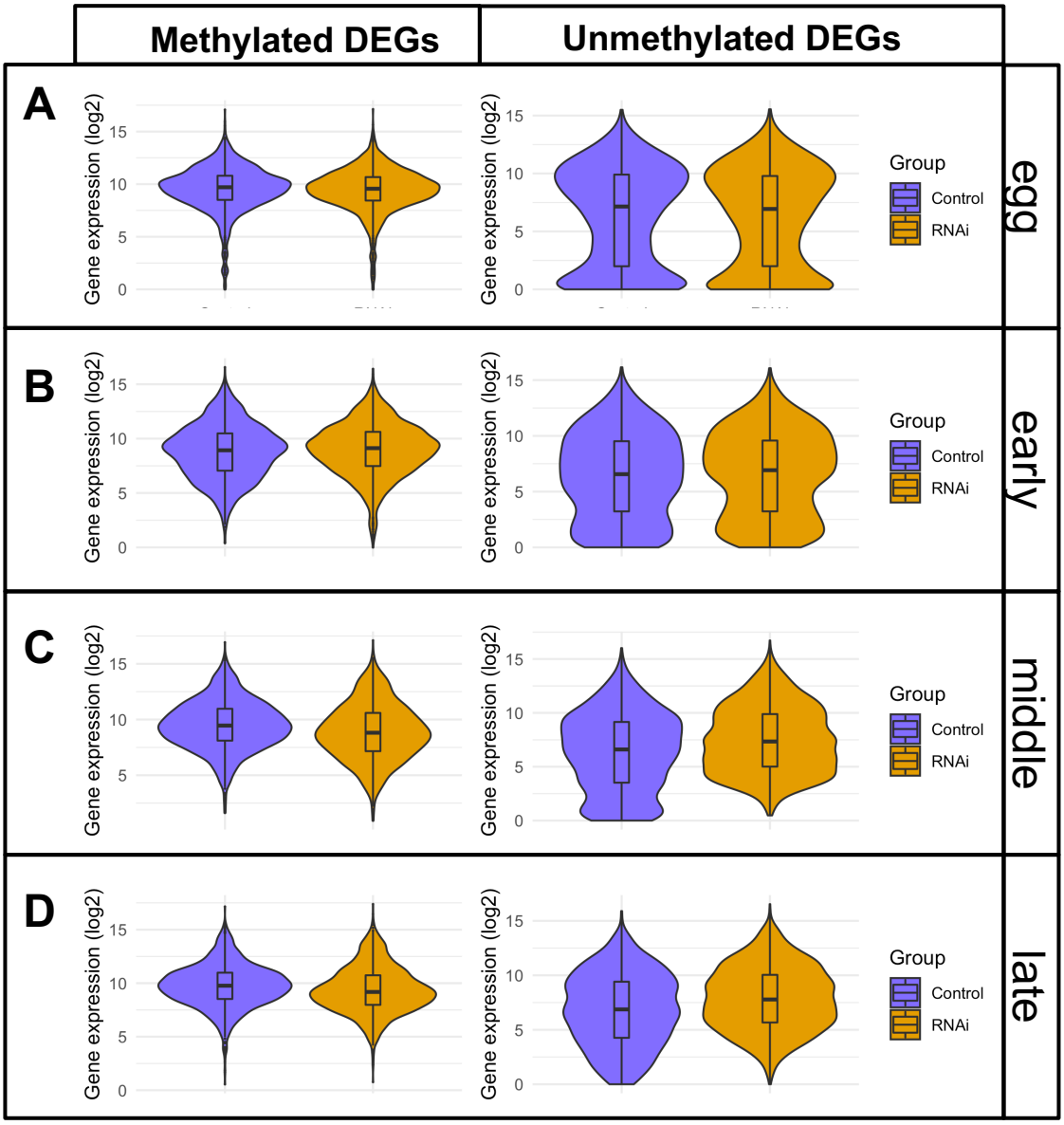
Methylated DEGs
Unmethylated DEGs
A
B
C
D
egg
early
middle
late
Gene expression (log2)
0
5
10
15
Group
Control
RNAi

Figure 6

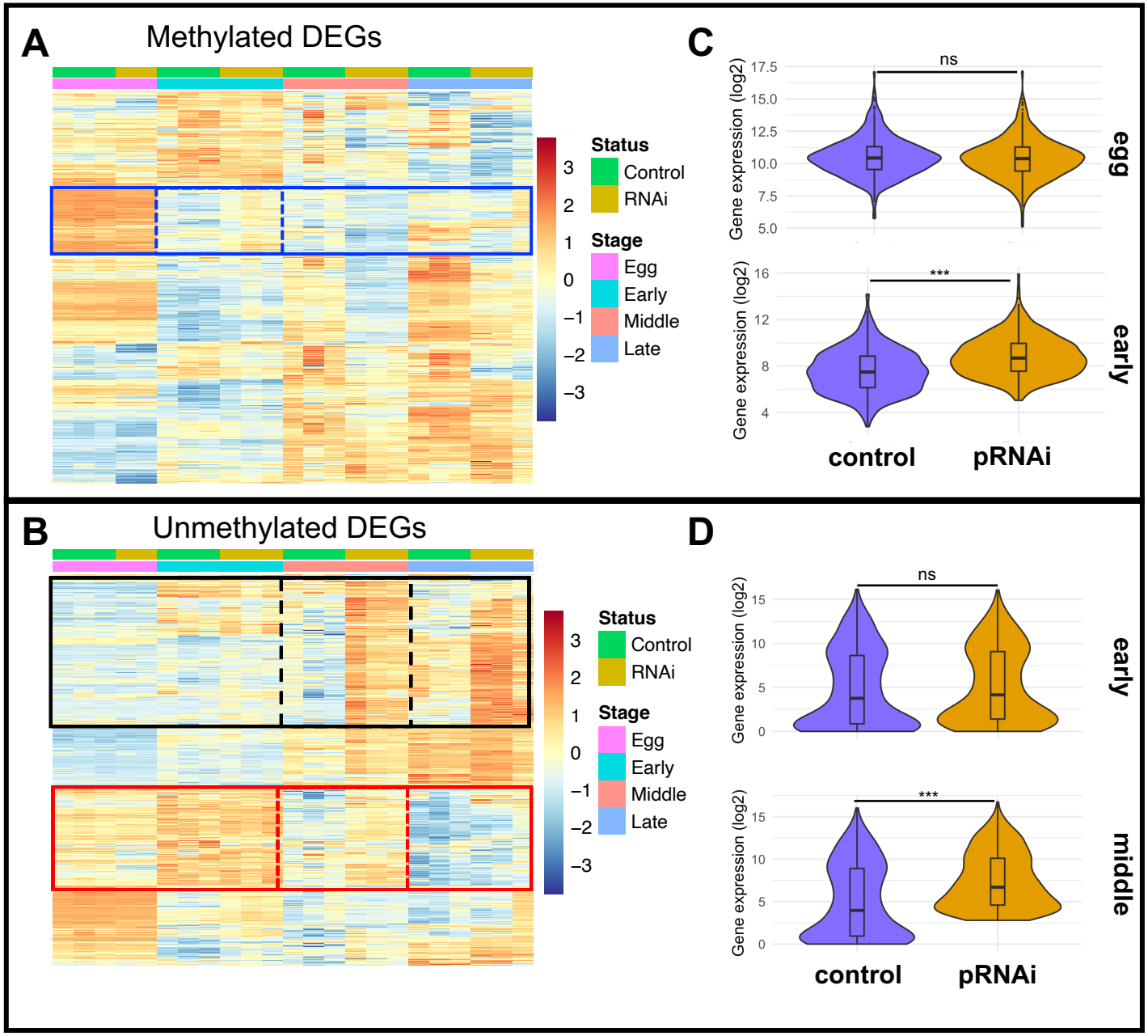
A
Methylated DEGs
Status
Control
RNAi
Stage
Egg
Early
Middle
Late
3
2
1
0
−1
−2
−3
C
ns
egg
***
early
Gene expression (log2)
control
pRNAi
B
Unmethylated DEGs
D
ns
early
***
middle

Suppl. Figure 1

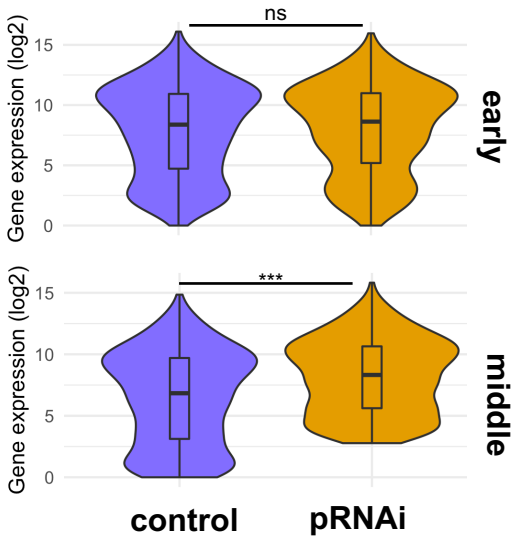

Category	Enriched terms	Count	%	P-Value	Benjamini
KEGG_PATHWAY	RNA degradation	16	2.1	0.00018	0.014
KEGG_PATHWAY	Oxidative phosphorylation	28	2.4	0.00064	0.032
KEGG_PATHWAY	Proteasome	16	1.4	0.00061	0.059
KEGG_PATHWAY	Basal transcription factors	10	1.3	0.0032	0.083
KEGG_PATHWAY	Endocytosis	21	2.7	0.0016	0.063
COG_ONTOLOGY	Translation, ribosomal structure and biogenesis	10	1.3	0.0023	0.044

Supplementary Table 1. GO Analysis for down-regulated methylated genes in middle and late blastoderm Nv-dnmt1a RNAi embryos